New rate coefficients of CS in collision with para- and ortho-H2 and astrophysical implications

Otoniel Denis-Alpizar, Thierry Stoecklin, S. Guilloteau, Anne Dutrey

Monthly Notices
of the
ROYAL ASTRONOMICAL SOCIETY

MNRAS **478,** 1811–1817 (2018)
Advance Access publication 2018 May 5

doi:10.1093/mnras/sty1177

New rate coefficients of CS in collision with para- and ortho-H_2 and astrophysical implications

Otoniel Denis-Alpizar,[1]★ Thierry Stoecklin,[2]★ Stéphane Guilloteau[3]★ and Anne Dutrey[3]

[1]*Facultad de Ingeniería, Instituto de Ciencias Químicas Aplicadas, Universidad Autónoma de Chile, El Llano Subercaseaux 2801, 8910060 San Miguel, Santiago, Chile*
[2]*Institut des Sciences Moléculaires, Université de Bordeaux, CNRS UMR 5255, F-33405 Talence Cedex, France*
[3]*Laboratoire d'astrophysique de Bordeaux, Université de Bordeaux, CNRS, B18N, Allée Geoffroy Saint-Hilaire, F-33615 Pessac, France*

Accepted 2018 April 24. Received 2018 April 17; in original form 2018 March 12

ABSTRACT

Astronomers use the CS molecule as a gas mass tracer in dense regions of the interstellar medium, to measure either the gas density through multiline observations or the level of turbulence. This necessarily requires the knowledge of the rates coefficients with the most common colliders in the interstellar medium, He and H_2. In this work, the close coupling collisional rates are computed for the first 30 rotational states of CS in collision with para- and ortho-H_2 using a recent rigid rotor potential energy surface. Some radiative transfer calculations, using typical astrophysical conditions, are also performed to test this new set of data and to compare with the existing ones.

Key words: astrochemistry – molecular data – molecular processes – scattering – ISM: molecules.

1 INTRODUCTION

Carbon monosulfide (CS) was among the first molecules detected in galactic (Martin & Barrett 1975; Zuckerman et al. 1976; Drdla, Knapp & Van Dishoeck 1989; Sánchez Contreras, Bujarrabal & Alcolea 1997; Agúndez et al. 2012) and extragalactic regions (Henkel & Bally 1985). Its strong dipole moment of 1.98 debye (Nelson, Lide & Maryott 1967) makes CS an excellent tracer of dense molecular gas in the interstellar medium (ISM) such as molecular clouds. In particular, CS multiline studies appear to be efficient to determine the gas structure in protoplanetary discs (Dutrey et al. 2017), where planets are expected to form, provided its collisional rates with H_2 (the main collider in dense molecular regions) are accurately known. Thanks to its high molecular mass ($\mu = 44$) compared to other molecules detected in discs, CS is also used to measure the level of turbulence. This method has been successfully applied to several proto-planetary discs such as DM Tau (Guilloteau et al. 2012) or TW Hydra (Teague et al. 2016).

Moreover, the advent of the new generation of mm capabilities, such as ALMA (Atacama Large Millimeter Array), reduces the observational uncertainties. Therefore, high-precision collisional rates with H_2 and He are necessary in the absence of local thermal equilibrium.

The only sets of data available in the literature are those of Turner et al. (1992) and Lique & Spielfiedel (2007) for the collision of CS with He and those of Denis-Alpizar et al. (2013) for the collisions of CS with H_2. These studies, unfortunately, included only the first 15 rotational states of CS while data for excited rotational states of CS up to 30 are needed to model some warmer environments of the ISM. In the later work of Denis-Alpizar et al. (2013) a comparison was done between the mass-scaled rates determined by Turner et al. (1992) or by Lique & Spielfiedel (2007) for CS-He and those computed by Denis-Alpizar et al. (2013) for CS-para-H_2. While this scaling approximation is known to fail in many cases, rate coefficients for a molecule in collision with para-H_2 are often estimated from those calculated for the collision with He (Schöier et al. 2005). Computer time saving is a great advantage offered by this approximation, but nevertheless, it cannot be used to predict the rate coefficients with ortho-H_2. While the scaled results of Lique & Spielfiedel (2007) and those of Denis-Alpizar et al. (2013) showed an overall agreement, a factor of 2 was observed with the results of Turner et al. (1992). This difference can be understood by comparing the *ab initio* and dynamics methods used in these different studies. The oldest work of Turner et al. (1992) was based on a simple electron gas model and used the coupled states approximation, while those of Lique & Spielfiedel (2007) for He-CS and Denis-Alpizar et al. (2013) for CS-H_2 were based on close coupling calculations and a high-level *ab initio* approach.

In this work, we compute the rates coefficients of CS in collision with para- and ortho-H_2 for the first 30 rotational states of CS. This

★ E-mail: otoniel.denis@uautonoma.cl (OD-A); thierry.stoecklin@u-bordeaux.fr (TS); Stephane.Guilloteau@u-bordeaux.fr (SG)

increment in the number of the collisional rates should allow a better determination of the density, molecular abundance, and excitation temperatures in the regions of the ISM where CS is observed. We furthermore perform radiative transfer calculations to test the effect of this new set of data on predicted density and temperature.

This article is organized as follows: in the next section, we describe the method used, while in Section 3 the main results are presented. In this later section, the new collisional rates are reported, and a preliminary study of their impact on predicted density and temperature is discussed. Finally, Section 4 summarizes this work.

2 METHODOLOGY

The collision of CS with H_2 is treated considering both diatoms as rigid rotors. This approximation is valid for collision energies lower than the vibrational frequency of the molecules involved (Stoecklin et al. 2017). We use the potential energy surface (PES) which we developed in our previous work dedicated to this system (Denis-Alpizar et al. 2012). This 4D surface is based on a large grid of *ab initio* points calculated at the CCSD(T) level using an aug-cc-pVQZ basis set complemented by bond functions. The energy grid was fitted to an analytical form, described in detail in the previous work, giving special attention to describe accurately the asymptotic long-range behaviour.

The dynamics of the system was performed using the DIDIMAT code (Guillon et al. 2008). The close coupling equations were solved in the space-fixed frame using the *R*-matrix propagator (Parker, Schmalz & Light 1980) and the rigid rotor approximation for collision energies ranging from 10^{-2} up to 3000 cm^{-1}. The rotational constants of the diatoms were fixed to their experimental values B_{CS}= 0.820 0462 cm^{-1} and B_{H_2} = 60.853 cm^{-1}. The propagation was carried out up to a maximum distance of $100a_0$ for the lowest energy considered in the calculations and the convergence was checked as a function of the total angular momentum for each collision energy.

30 rotational states of CS were included in the rotational basis set for transitions starting from initial rotational states of CS J^i_{CS} lower than 20, while for $21 \leq J^i_{CS} \leqslant 30$, $J^i_{CS} + 10$ rotational levels of CS were included in the rotational basis set. We furthermore showed in our previous work dedicated to this system (Denis-Alpizar et al. 2013) that adding a second rotational function to the rotational basis set of H_2 changes the values of the cross-sections by 4 per cent at the most. Therefore, only one rotational level of H_2 was included in the basis set to reduce computer time. The state-to-state rate coefficients were eventually determined by Boltzmann averaging the corresponding cross-sections over collision energy.

3 RESULTS

3.1 Rate coefficients

The J^f_{CS} dependence of the rate coefficients for the rotational de-excitation of CS ($J^i_{CS} = 21$) in collisions with para-H_2 ($J_{H_2} = 0$) and ortho-H_2 ($J_{H_2} = 1$) are shown in Fig. 1 for the three temperatures T= 10, 100, and 300 K. On the same figure, the present para-H_2-CS data are also compared with those obtained from mass scaling the He-CS rate coefficients (Lique & Spielfiedel 2007). If the order of magnitude of the state-to-state rate coefficients appears to be approximately predicted by the mass-scaling approximation for odd transitions, it is not for the even transitions. This approximation also fails reproducing the propensity rules to favour even ΔJ transitions

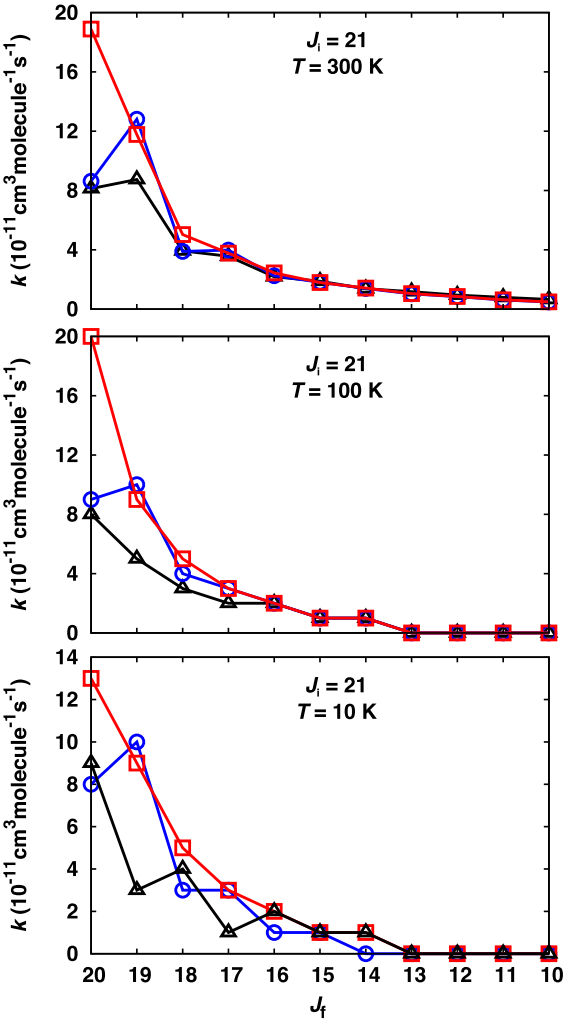

Figure 1. J^f_{CS} dependence of the rotational de-excitation rate coefficients of CS ($J_{CS} = 21$) in collision with para-H_2 (blue solid lines) and ortho-H_2 (red solid lines) at $T = 10$ K. The para-H_2-CS rate coefficients obtained by Denis-Alpizar et al. (2013) from mass scaling the He-CS rate coefficients are also shown (black lines).

for large values of J^i_{CS} at any temperature. For transitions issued from lower rotational states J^i_{CS} (up to $J^i_{CS} = 10$), the same even propensity rule was found to hold at low T and to reverse at higher temperatures (Denis-Alpizar et al. 2013). This is in contrast with the collisions with ortho-H_2 for which the CS rotational de-excitation rates monotonously decrease when ΔJ increases for all the values of J^i_{CS} considered in our calculations and at any temperature.

Tables 1 and 2 show, respectively, the collisional rates coefficients of CS in collision with para-H_2 and ortho-H_2 at selected temperatures for two initial values of the rotational angular momentum of CS: ($J^i_{CS} = 16$ and 17). The values computed by Denis-Alpizar et al. (2013) for the first 15 rotational states of CS and the full table of those computed here for values of J^i_{CS} up to 29 from 5 to 305 K are reported in the supplementary materials. The complete set of rates will also be available on the Basecol data base (http://basecol.obspm.fr, Dubernet et al. 2013). This new set of rotational de-excitation rate coefficients of CS colliding with H_2, together with those already available for the collision with He (Lique & Spielfiedel 2007), should help in improving the model of abundance of CS in the ISM.

Table 1. Rotational de-excitation rate coefficients (cm^3 $molecule^{-1}$ s^{-1}) of CS in collision with para-H_2 ($J_{H_2} = 0$) at selected temperatures. Full table with the rates of CS in collision with para-H_2 can be found in supplementary materials.

Transition		Temperature (K)					
J^i_{CS}	J^f_{CS}	10.1	20.6	40.6	80.6	100.6	205.6
16	0	2.5×10^{-15}	3.6×10^{-15}	6.2×10^{-15}	1.7×10^{-14}	2.7×10^{-14}	1.1×10^{-13}
16	1	1.3×10^{-14}	1.7×10^{-14}	2.7×10^{-14}	6.6×10^{-14}	9.6×10^{-14}	3.4×10^{-13}
16	2	3.3×10^{-14}	4.4×10^{-14}	6.7×10^{-14}	1.5×10^{-13}	2.1×10^{-13}	6.4×10^{-13}
16	3	9.0×10^{-14}	1.1×10^{-13}	1.6×10^{-13}	3.1×10^{-13}	4.1×10^{-13}	1.1×10^{-12}
16	4	2.1×10^{-13}	2.6×10^{-13}	3.5×10^{-13}	6.1×10^{-13}	7.7×10^{-13}	1.7×10^{-12}
16	5	4.6×10^{-13}	5.5×10^{-13}	7.1×10^{-13}	1.1×10^{-12}	1.3×10^{-12}	2.5×10^{-12}
16	6	1.0×10^{-12}	1.2×10^{-12}	1.4×10^{-12}	2.0×10^{-12}	2.3×10^{-12}	3.7×10^{-12}
16	7	2.0×10^{-12}	2.3×10^{-12}	2.6×10^{-12}	3.4×10^{-12}	3.7×10^{-12}	5.4×10^{-12}
16	8	3.7×10^{-12}	4.2×10^{-12}	4.7×10^{-12}	5.5×10^{-12}	5.9×10^{-12}	7.4×10^{-12}
16	9	6.6×10^{-12}	7.2×10^{-12}	7.6×10^{-12}	8.3×10^{-12}	8.7×10^{-12}	1.0×10^{-11}
16	10	1.1×10^{-11}	1.2×10^{-11}	1.3×10^{-11}	1.3×10^{-11}	1.3×10^{-11}	1.4×10^{-11}
16	11	1.6×10^{-11}	1.7×10^{-11}	1.7×10^{-11}	1.7×10^{-11}	1.7×10^{-11}	1.8×10^{-11}
16	12	3.0×10^{-11}	3.2×10^{-11}	3.1×10^{-11}	3.0×10^{-11}	2.9×10^{-11}	3.2×10^{-11}
16	13	3.5×10^{-11}	3.7×10^{-11}	3.6×10^{-11}	3.4×10^{-11}	3.4×10^{-11}	3.3×10^{-11}
16	14	1.0×10^{-10}	1.1×10^{-10}	1.1×10^{-10}	1.0×10^{-10}	1.1×10^{-10}	1.2×10^{-10}
16	15	1.1×10^{-10}	1.1×10^{-10}	1.0×10^{-10}	9.2×10^{-11}	9.0×10^{-11}	8.5×10^{-11}
17	0	1.5×10^{-15}	2.1×10^{-15}	3.7×10^{-15}	1.1×10^{-14}	1.7×10^{-14}	7.3×10^{-14}
17	1	6.0×10^{-15}	8.5×10^{-15}	1.4×10^{-14}	3.8×10^{-14}	5.8×10^{-14}	2.4×10^{-13}
17	2	2.0×10^{-14}	2.7×10^{-14}	4.0×10^{-14}	9.2×10^{-14}	1.3×10^{-13}	4.5×10^{-13}
17	3	4.9×10^{-14}	6.4×10^{-14}	9.3×10^{-14}	1.9×10^{-13}	2.6×10^{-13}	7.7×10^{-13}
17	4	1.2×10^{-13}	1.5×10^{-13}	2.1×10^{-13}	3.8×10^{-13}	4.9×10^{-13}	1.2×10^{-12}
17	5	2.8×10^{-13}	3.4×10^{-13}	4.5×10^{-13}	7.3×10^{-13}	9.1×10^{-13}	1.9×10^{-12}
17	6	5.7×10^{-13}	6.9×10^{-13}	8.6×10^{-13}	1.3×10^{-12}	1.5×10^{-12}	2.8×10^{-12}
17	7	1.2×10^{-12}	1.4×10^{-12}	1.7×10^{-12}	2.3×10^{-12}	2.6×10^{-12}	4.0×10^{-12}
17	8	2.3×10^{-12}	2.6×10^{-12}	3.0×10^{-12}	3.7×10^{-12}	4.1×10^{-12}	5.8×10^{-12}
17	9	4.2×10^{-12}	4.8×10^{-12}	5.2×10^{-12}	6.0×10^{-12}	6.4×10^{-12}	7.9×10^{-12}
17	10	7.0×10^{-12}	7.9×10^{-12}	8.3×10^{-12}	9.0×10^{-12}	9.3×10^{-12}	1.1×10^{-11}
17	11	1.2×10^{-11}	1.3×10^{-11}	1.4×10^{-11}	1.4×10^{-11}	1.4×10^{-11}	1.5×10^{-11}
17	12	1.6×10^{-11}	1.8×10^{-11}	1.8×10^{-11}	1.8×10^{-11}	1.8×10^{-11}	1.9×10^{-11}
17	13	3.1×10^{-11}	3.3×10^{-11}	3.2×10^{-11}	3.0×10^{-11}	3.0×10^{-11}	3.3×10^{-11}
17	14	3.6×10^{-11}	3.9×10^{-11}	3.8×10^{-11}	3.5×10^{-11}	3.5×10^{-11}	3.4×10^{-11}
17	15	1.0×10^{-10}	1.1×10^{-10}	1.1×10^{-10}	1.1×10^{-10}	1.1×10^{-10}	1.2×10^{-10}
17	16	1.1×10^{-10}	1.1×10^{-10}	1.0×10^{-10}	9.2×10^{-11}	9.0×10^{-11}	8.5×10^{-11}

3.2 Astrophysical implications

In this section, we evaluate the impact of the new collision rates on the determination of astrophysical parameters. This impact will depend on the ortho-to-para ratio of H_2, since the collision rates of CS with these two forms of H_2 differ by factors of order 2.

We first simulated with a large velocity gradient (LVG) radiative transfer code the emission coming from a region of temperature 20 K, density 10^6 cm^{-3}, and CS column density 10^{13} cm^{-2} for a linewidth of 0.3 $km\,s^{-1}$. We used three different choices for the collision rates: those derived from the CS-He study of Lique & Spielfiedel (2007), scaled for the different mass of H_2 as available in the LAMDA data base (Schöier et al. 2005) (`lamda` rates), rates for CS with para-H_2 [as would be appropriate at low temperatures if conversion between the two H_2 spin states occurs (`para` rates)], and rates assuming an ortho to para ratio for H_2 equal to 3, the statistical value (`normal` rates). The ortho–para ratio can be different from one astrophysical medium to another (Pagani, Daniel & Dubernet 2009; Crabtree et al. 2011; Brünken et al. 2014) and its value is conditioned by several processes (Bron, Le Petit & Le Bourlot 2016). We explore here the two most extreme cases.

The predicted intensities of a set of selected transitions were then fitted using the same LVG code with the `lamda` rates, after allowing for a relative error ϵ on the predicted brightnesses. This relative error mimics the absolute calibration uncertainty that is unavoidable in the observations. The transitions selected for the analysis were J= 3–2, J= 5–4,and J= 7–6 lines, and another study was made with the J= 2–1 line in addition. We determined which temperature, density, and column density triplet could best reproduce the measurement and with what typical error. We used a Monte Carlo Markov Chain method to evaluate the error bars on each parameter. For this, we used the affine invariant method of Goodman & Weave (2010) as implemented in the PYTHON EMCEE package by Foreman-Mackey et al. (2013). The resulting posterior distributions of the parameters are presented in Fig. 2. Density and column density are in decimal log scale with uniform prior over a wide enough range [typically 1–10 for Log_{10}(density) and 10–16 for Log_{10}(column density)]. Temperature is linear with a uniform prior between 3 and 100 K.

In Fig. 2, top panel, the line intensities were simulated and fitted using the `lamda` rates. Not surprisingly, the input parameters are recovered but with an error distribution which reflects the assumed calibration error ϵ. In the middle panel, we used the `para` rates for the simulation and the `lamda` rates for the analysis. Here, the recovered solution is significantly different. The column density is correctly recovered. However, the best-fitting temperature is 20 per cent too low and the density is about two times too large. The later result is not surprising, since looking at the raw values of the collision rates there is indeed a factor of order 2 between the `lamda` rates and ours. The former result is more surprising as

Table 2. Rotational de-excitation rate coefficients (cm^3 $molecule^{-1}$ s^{-1}) of CS in collision with ortho-H_2 ($J_{H_2} = 1$) at selected temperatures. Full table with the rates of CS in collision with ortho-H_2 can be found in supplementary materials.

Transition		Temperature (K)					
J^i_{CS}	J^f_{CS}	10.1	20.6	40.6	80.6	100.6	205.6
16	0	4.4×10^{-15}	6.1×10^{-15}	9.7×10^{-15}	2.4×10^{-14}	3.4×10^{-14}	1.2×10^{-13}
16	1	1.9×10^{-14}	2.5×10^{-14}	3.9×10^{-14}	8.5×10^{-14}	1.2×10^{-13}	3.7×10^{-13}
16	2	5.2×10^{-14}	6.7×10^{-14}	9.6×10^{-14}	1.9×10^{-13}	2.5×10^{-13}	6.9×10^{-13}
16	3	1.3×10^{-13}	1.6×10^{-13}	2.2×10^{-13}	3.9×10^{-13}	4.9×10^{-13}	1.2×10^{-12}
16	4	3.0×10^{-13}	3.6×10^{-13}	4.6×10^{-13}	7.3×10^{-13}	8.9×10^{-13}	1.8×10^{-12}
16	5	6.4×10^{-13}	7.5×10^{-13}	9.2×10^{-13}	1.3×10^{-12}	1.5×10^{-12}	2.7×10^{-12}
16	6	1.3×10^{-12}	1.5×10^{-12}	1.7×10^{-12}	2.3×10^{-12}	2.6×10^{-12}	3.9×10^{-12}
16	7	2.5×10^{-12}	2.8×10^{-12}	3.1×10^{-12}	3.8×10^{-12}	4.1×10^{-12}	5.6×10^{-12}
16	8	4.4×10^{-12}	4.9×10^{-12}	5.2×10^{-12}	5.9×10^{-12}	6.2×10^{-12}	7.6×10^{-12}
16	9	7.5×10^{-12}	8.2×10^{-12}	8.5×10^{-12}	9.0×10^{-12}	9.2×10^{-12}	1.1×10^{-11}
16	10	1.2×10^{-11}	1.3×10^{-11}	1.3×10^{-11}	1.3×10^{-11}	1.3×10^{-11}	1.4×10^{-11}
16	11	1.9×10^{-11}	2.0×10^{-11}	2.0×10^{-11}	1.9×10^{-11}	1.9×10^{-11}	2.0×10^{-11}
16	12	2.8×10^{-11}	2.9×10^{-11}	2.9×10^{-11}	2.8×10^{-11}	2.8×10^{-11}	3.1×10^{-11}
16	13	5.0×10^{-11}	5.3×10^{-11}	5.2×10^{-11}	4.8×10^{-11}	4.7×10^{-11}	4.5×10^{-11}
16	14	9.0×10^{-11}	9.4×10^{-11}	9.4×10^{-11}	9.4×10^{-11}	9.5×10^{-11}	1.1×10^{-10}
16	15	1.6×10^{-10}	1.9×10^{-10}	2.0×10^{-10}	2.1×10^{-10}	2.0×10^{-10}	1.9×10^{-10}
17	0	2.4×10^{-15}	3.4×10^{-15}	5.6×10^{-15}	1.4×10^{-14}	2.1×10^{-14}	8.1×10^{-14}
17	1	1.0×10^{-14}	1.4×10^{-14}	2.2×10^{-14}	5.1×10^{-14}	7.4×10^{-14}	2.6×10^{-13}
17	2	3.0×10^{-14}	3.9×10^{-14}	5.7×10^{-14}	1.2×10^{-13}	1.6×10^{-13}	5.0×10^{-13}
17	3	7.4×10^{-14}	9.4×10^{-14}	1.3×10^{-13}	2.4×10^{-13}	3.2×10^{-13}	8.3×10^{-13}
17	4	1.8×10^{-13}	2.2×10^{-13}	2.8×10^{-13}	4.7×10^{-13}	5.9×10^{-13}	1.3×10^{-12}
17	5	3.8×10^{-13}	4.5×10^{-13}	5.7×10^{-13}	8.6×10^{-13}	1.0×10^{-12}	2.0×10^{-12}
17	6	7.8×10^{-13}	9.1×10^{-13}	1.1×10^{-12}	1.5×10^{-12}	1.8×10^{-12}	2.9×10^{-12}
17	7	1.5×10^{-12}	1.8×10^{-12}	2.0×10^{-12}	2.6×10^{-12}	2.9×10^{-12}	4.2×10^{-12}
17	8	2.8×10^{-12}	3.2×10^{-12}	3.5×10^{-12}	4.2×10^{-12}	4.5×10^{-12}	6.0×10^{-12}
17	9	4.8×10^{-12}	5.4×10^{-12}	5.8×10^{-12}	6.4×10^{-12}	6.7×10^{-12}	8.0×10^{-12}
17	10	8.1×10^{-12}	8.9×10^{-12}	9.2×10^{-12}	9.6×10^{-12}	9.8×10^{-12}	1.1×10^{-11}
17	11	1.2×10^{-11}	1.4×10^{-11}	1.4×10^{-11}	1.4×10^{-11}	1.4×10^{-11}	1.5×10^{-11}
17	12	1.9×10^{-11}	2.1×10^{-11}	2.1×10^{-11}	2.0×10^{-11}	2.0×10^{-11}	2.0×10^{-11}
17	13	2.8×10^{-11}	3.1×10^{-11}	3.0×10^{-11}	2.9×10^{-11}	2.9×10^{-11}	3.1×10^{-11}
17	14	5.0×10^{-11}	5.4×10^{-11}	5.3×10^{-11}	4.9×10^{-11}	4.8×10^{-11}	4.6×10^{-11}
17	15	9.2×10^{-11}	9.5×10^{-11}	9.5×10^{-11}	9.4×10^{-11}	9.6×10^{-11}	1.1×10^{-10}
17	16	1.6×10^{-10}	1.8×10^{-10}	2.0×10^{-10}	2.1×10^{-10}	2.0×10^{-10}	2.0×10^{-10}

even the measured temperature seems to be wrong. In the lower panel, we used the `normal` rates for the simulation (i.e. H_2 with an ortho–para ratio of 3:1) and the `lamda` rates for the analysis. The effect seen with para H_2 is now even more pronounced and a second, high-density but low-temperature, regime becomes possible.

Fig. 2 used a relative error $\epsilon = 1$ per cent to better illustrate the systematic differences. However, more realistic calibration accuracies are in the range 5–10 per cent (ALMA has an absolute accuracy goal of 3 per cent). Fig. 3 shows what happens with a $\epsilon = 6$ per cent relative error. This larger (yet typical or even optimistic) relative error considerably modifies the allowed range of solutions. In addition to those found before, solutions with even lower temperatures and higher column density become possible as well as solutions with high densities. These branches of possible solutions can be suppressed to some extent by considering also the J= 2–1 line in the analysis, as shown in Fig. 4, especially for the ortho-to-para ratio equals to 3. Of course, at higher densities the impact of the collision rates will be less severe since all lines will get closer to thermalization.

Results for conditions more appropriate for cold clouds, $n(H_2) = 10^5\,cm^{-3}$, $T = 12$ K, and $N(CS) = 10^{13}\,cm^{-2}$ are shown in Fig. 5. Here, a plateau of solutions which are degenerate between density and column density appears: collisional excitation can be traded against radiative trapping. A prior knowledge of the kinetic temperature does not solve this fundamental behaviour. The degeneracy can only be removed if the column density of CS is determined separately, either adding the more optically thin J= 1–0 line or using observations of other isotopologues, e.g. $C^{34}S$. In that case, the temperature fitted using the scaled He rates will, however, underestimate the true value by about 15 per cent.

4 SUMMARY

The rotational de-excitation rate coefficients of CS by collision with para-H_2 and ortho-H_2 were calculated at the close coupling level and within the rigid rotor approximation for the 30 first rotational states of CS. These calculations used our recently developed 4D PES based on a large grid of CCSD(T)/aug-cc-pVQZ+bf *ab initio* points. The present para-H_2-CS data are also compared with those obtained by Lique & Spielfiedel (2007) from mass scaling the He-CS rate coefficients. If the order of magnitude of the state-to-state rate coefficients appears to be approximately predicted by the mass-scaling approximation for odd transitions, it is not for the even transitions. This approximation also fails reproducing the propensity rules to favour even ΔJ transitions for large values of J^i_{CS} at any temperature. For transitions issued from lower rotational states J^i_{CS} (up to $J^i_{CS} = 10$), the same even propensity rule was found to hold at low T and to reverse at higher temperatures (Denis-Alpizar et al.

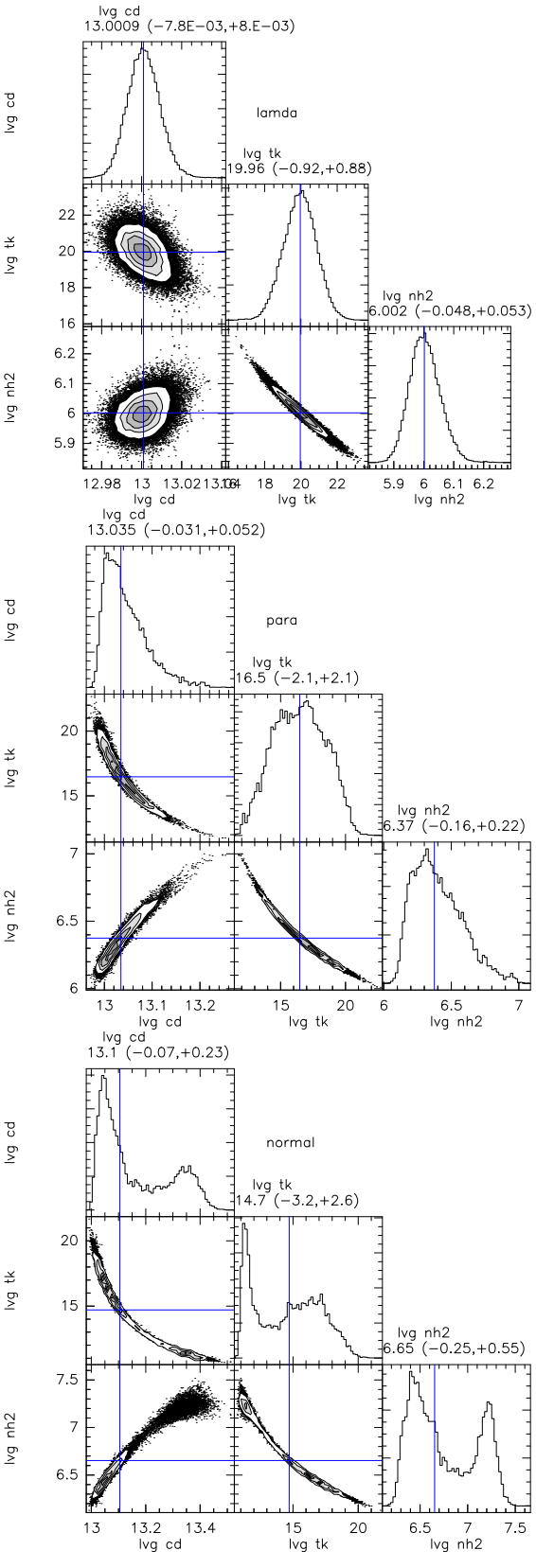

Figure 2. Correlation plots of the distribution of temperature, density, and column density predicted using (from top to bottom) the rates from the Lamda data base (`lamda`), the new rates for para H_2 (`para`), or the rates for H_2 with an ortho-to-para ratio of 3 (`normal`). A 1 per cent measurement error is considered.

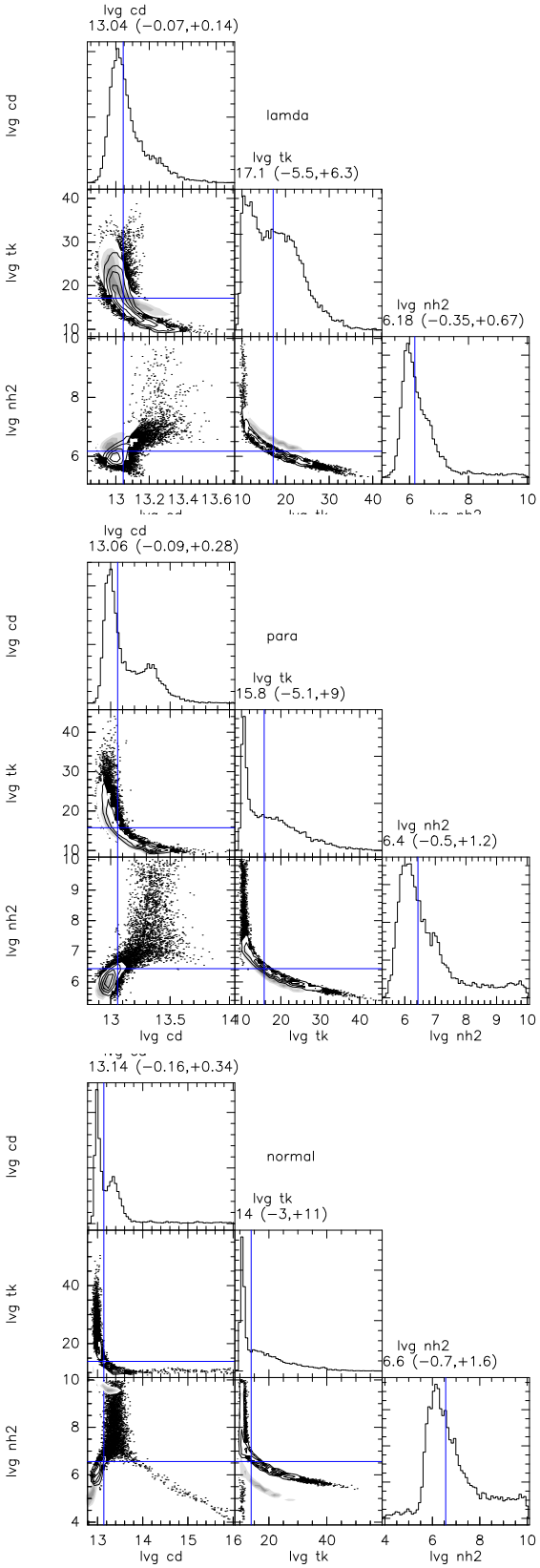

Figure 3. As Fig. 2, but for a 6 per cent measurement error.

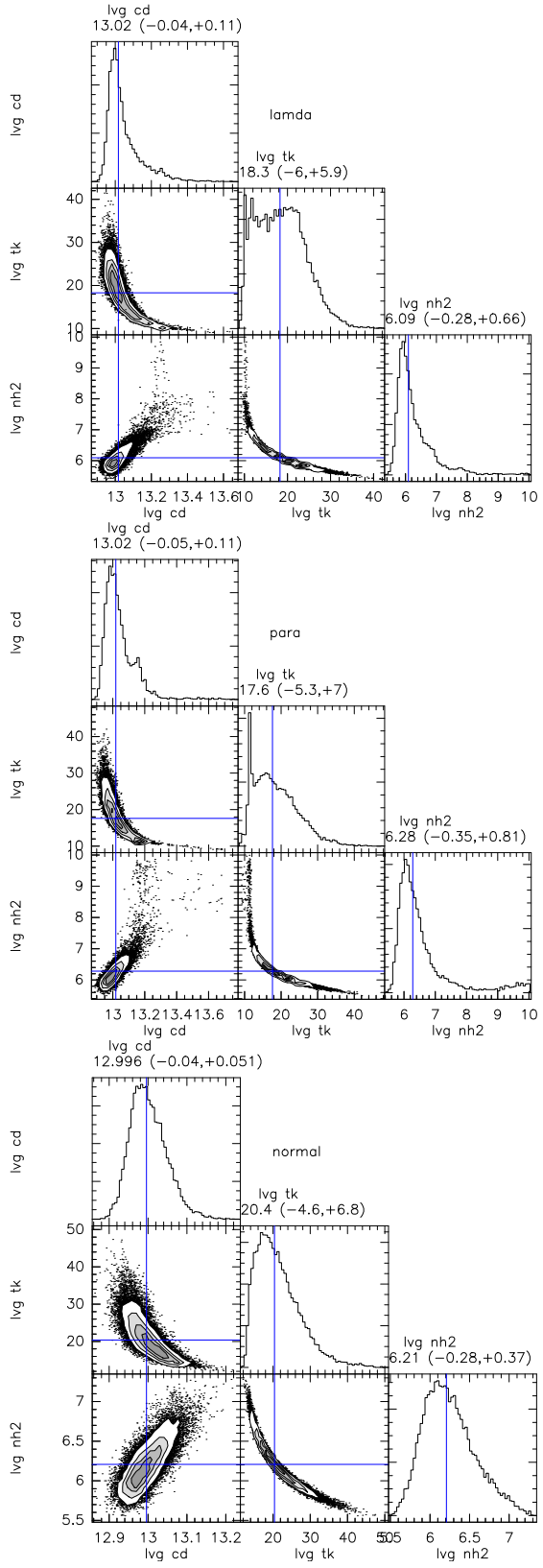

Figure 4. As Fig. 3, but using also the $J = 2$–1 line in the fitting process.

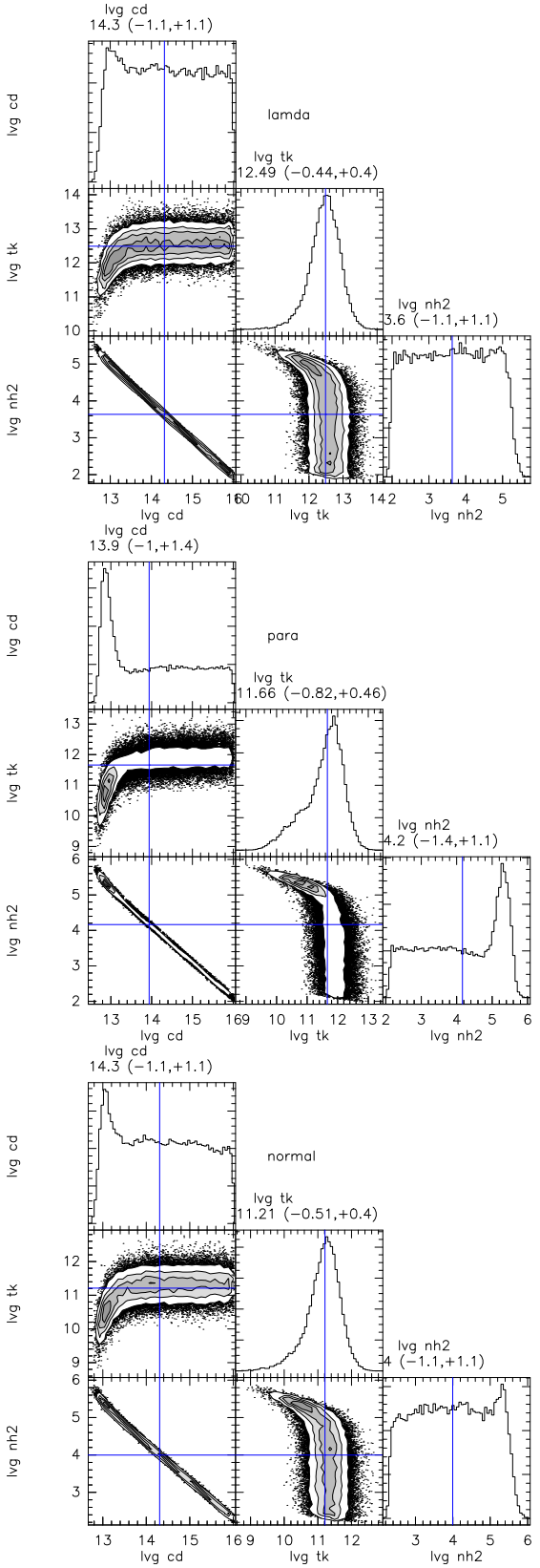

Figure 5. As Fig. 3, but for conditions more appropriate to dense cores and using the $J = 2$–1, 3–2,and 5–4 lines only.

2013). This is in contrast with the collisions with ortho-H_2 for which the CS rotational de-excitation rates monotonously decrease when ΔJ increases for all the values of J^i_{CS} considered in our calculations and at any temperature.

The difference between these new collision rates and the scaled He rates significantly impacts the determination of physical parameters from CS multitransition observations. When using the scaled He rates, densities are typically overestimated by a factor 2, but the derived temperatures could be significantly in error.

ACKNOWLEDGEMENTS

Computer time for this study was provided by the Mésocentre de Calcul Intensif Aquitain which is the computing facility of Université de Bordeaux et Université de Pau et des Pays de l'Adour. This work was supported by the Programme National 'Physique et Chimie du Milieu Interstellaire' (PCMI) of CNRS/INSU with INC/INP and co-funded by CEA and CNES. ODA acknowledges the support from the project CONICYT/FONDECYT/INICIACION/No.11160005.

REFERENCES

Agúndez M., Fonfría J. P., Cernicharo J., Kahane C., Daniel F., 2012, A&A, 543, A48
Bron E., Le Petit F., Le Bourlot J., 2016, A&A, 588, A27
Brünken S. et al., 2014, Nature, 516, 219
Crabtree K. N., Indriolo N., Kreckel H., Tom B. A., McCall B. J., 2011, ApJ, 729, 15
Denis-Alpizar O., Stoecklin T., Halvick P., Dubernet M., Marinakis S., 2012, J. Chem. Phys., 137, 234301
Denis-Alpizar O., Stoecklin T., Halvick P., Dubernet M.-L., 2013, J. Chem. Phys., 139, 204304
Drdla K., Knapp G., Van Dishoeck E., 1989, ApJ, 345, 815
Dubernet M.-L. et al., 2013, A&A, 553, A50
Dutrey A. et al., 2017, A&A, 607, A130
Foreman-Mackey D., Hogg D. W., Lang D., Goodman J., 2013, PASP, 125, 306
Goodman J., Weave J., 2010, Commun. Appl. Math. Comput. Sci., 5, 65
Guillon G., Stoecklin T., Voronin A., Halvick P., 2008, J. Chem. Phys., 129, 104308
Guilloteau S., Dutrey A., Wakelam V., Hersant F., Semenov D., Chapillon E., Henning T., Piétu V., 2012, A&A, 548, A70
Henkel C., Bally J., 1985, A&A, 150, L25
Lique F., Spielfiedel A., 2007, A&A, 462, 1179
Martin R., Barrett A., 1975, ApJ, 202, L83
Nelson R. D., Jr, Lide D. R., Jr, Maryott A. A., 1967, Technical report, Selected values of electric dipole moments for molecules in the gas phase. DTIC Document
Pagani L., Daniel F., Dubernet M.-L., 2009, A&A, 494, 719
Parker G. A., Schmalz T. G., Light J. C., 1980, J. Chem. Phys., 73, 1757
Sánchez Contreras C., Bujarrabal V., Alcolea J., 1997, A&A, 327, 689
Schöier F. L., van der Tak F. F. S., van Dishoeck E. F., Black J. H., 2005, A&A, 432, 369
Stoecklin T., Faure A., Jankowski P., Chefdeville S., Bergeat A., Naulin C., Morales S., Costes M., 2017, Phys. Chem. Chem. Phys., 19, 189
Teague R. et al., 2016, A&A, 592, A49
Turner B. E., Chan K.-W., Green S., Lubowichl D.-A., 1992, ApJ, 399, 114
Zuckerman B., Gilra D., Turner B., Morris M., Palmer P., 1976, ApJ, 205, L15

SUPPORTING INFORMATION

Supplementary data are available at *MNRAS* online.

rates_cs-paraH2.txt
rates_cs-orthoH2.txt

Please note: Oxford University Press is not responsible for the content or functionality of any supporting materials supplied by the authors. Any queries (other than missing material) should be directed to the corresponding author for the article.

This paper has been typeset from a TEX/LATEX file prepared by the author.